Modelling of carbon nanotube-based devices: from nanoFETs to THz emitters

Aldo Di Carlo, Alessandro Pecchia, Eleonora Petrolati, Claudio Paoloni

Dept. Electronic Eng., University of Rome "Tor Vergata", via del Politecnico 1, 00133 Roma,
dicarlo@ing.uniroma2.it

ABSTRACT

In the first part of the present contribution, we will report on transport calculations of nanoscaled devices based on Carbon Nanotubes obtained via self-consistent density-functional method coupled with non-equilibrium Green's function approaches. In particular, density functional tight-binding techniques are very promising due to their intrinsic efficiency. This scheme allows treatment of systems comprising a large number of atoms and enables the computation of the current flowing between two or more contacts in a fully self-consistent manner with the open boundary conditions that naturally arise in transport problems. We will give a description of this methodology and application to field effect transistor based on Carbon nanotubes.

The advances in manufacturing technology are allowing new opportunities even for vacuum electron devices producing radio-frequency radiation. Modern micro and nano-technologies can overcome the typical severe limitations of vacuum tube devices. As an example, Carbon Nanotubes used as cold emitters in micron-scaled triodes allow for frequency generation up to THz region. The purpose of the second part of this contribution will be a description of the modelling of Carbon Nanotube based vacuum devices such as triodes. We will present the calculation of important figures of merit and possible realizations.

Keywords: Carbon Nanotubes, Non-equilibrium Green Functions, Density Functional Theory, Quantum Transport, THz, PIC

INTRODUCTION

Technological advances in fabrication, characterization and control at the nanoscale level have enabled the manufacturing of a variety of new organic-inorganic nanostructured devices with a good degree of reproducibility. Such a new class of devices requires new simulation approaches, since the inherent quantum-mechanical physics involved must be treated properly and the exact nature of the transport mechanisms in many of such systems still remains open.
Carbon nanotubes have been recently acknowledged as promising candidates, among several low-dimensional physical systems, to realize nanoscale electronic devices [3], [4]. In particular, single-wall CNTs, consisting of a single graphene sheet wrapped up to form tubes with very small diameters, are ideal candidates to study general transport properties of quasi-one dimensional devices. CNTs posses exceptional electrical and mechanical properties, such as an exceptional strength and stability, which generate in turn the capability of carrying very high current densities [5]; very large values of the mean free path have been found, which guarantee carriers to propagate ballistically over very long distances even at room temperature (~ 1 μm in the low field regime) [6]. A CNT can be either metallic or semiconducting, depending on its chirality. Metallic CNTs can be employed as good interconnections among electrical devices at the nanoscale. Semiconducting CNTs have been instead used to demonstrate field-effect transistors having quasi-one dimensional channels [7].
The simplest approach to realize a nanotube transistor consists of contacting a semiconducting nanotube with two metallic contacts acting as source and drain. A gate modulates the injection of carriers in the nanotube channel by modulating the barrier height at the metal-semiconductor interface. A Schottky barrier (SB) nanotube transistor results in this case [8]. Significant progresses have been made in the fabrication and the understanding of these kind of devices. A SB-CNT transistor is essentially governed by a contactdominated switching. This is the fundamental difference with respect to conventional MOSFET devices, governed by conductance modulation of the channel. Indeed, SB-modulation strongly affects the performances of the nanotube device. The contact-dominated control mechanism leads to a large sub-threshold swing $S = dV_G/d(\log I_{DS})$ (where V_G and I_{DS} are respectively the gate voltage and the source-drain

Nanomodeling II, edited by Akhlesh Lakhtakia, Sergey A. Maksimenko,
Proc. of SPIE Vol. 6328, 632808, (2006) · 0277-786X/06/$15 · doi: 10.1117/12.680305

current), substantially limiting the gate insulator thinning, since a strong ambipolar behavior appears when the device is vertically scaled [8], [9], [10]. These drawbacks can prevent nanotube transistors from holding particular promises for highperformance nano-electronics.

Recently, novel device configurations for bulk-switched CNTFETs have been proposed and demonstrated [1], [2]. To obtain a channel-dominated behavior, a local gate contact is realized in the middle point of the channel, strongly reducing electrostatic coupling with the source and drain contacts [11].

The height of the contacts barrier simply fixes the charge injected in the channel, regardless the value set for the gate bias. The carrier injection can be controlled either by electrostatic or chemical doping of the ungated portion of the nanotube [2]. This device scheme allows to greatly improve the nanotube transistor performances. A transition from ambipolar to unipolar behavior has been demonstrated. Moreover, measured devices have shown a very small sub-threshold swing, very close to the theoretical limit found for standard MOSFET, and an excellent I_{on}/I_{off} ratio. Nevertheless, important issues need still to be addressed for the bulk-switched CNTFET. The conductance modulation mechanism involved in the device behavior is obtained by locally modulating the barrier height for carrier transmission through the nanotube. Consequently, local screening properties of the quasi-one dimensional electron gas associated to the nanotube can assume a predominant role in the switching mechanism.

Beside electronic applications, CNT can been very useful as field emitter even for THz sources. THz technology and applications have long been the field of molecular astronomers and chemical spectroscopists. However, recent advances in THz detectors and sources have started to open the field to new applications, including measurement systems, biological and medical applications, material characterisation and security.

The most difficult component to realize in the submillimeter wave bands has been the THz source. The submillimeter and terahertz regions are areas where electron mobility in semiconductors cannot meet the specifications. These specification, however, can be achieved with electrons travelling in vacuum, assuming the electric and magnetic fields can be shaped to modulate the beams and convert their energy to RF power.

Vacuum device technology is well established for obtaining high output power up to millimeter wave frequency. Conventional vacuum tubes include thermionic cathodes for generating an electron beam of adequate characteristics operating at high temperature (800 ^{O}C-1200°C).

The introduction of FEA (field emission array) cathode offers significant advantage for THz frequency amplification. Further, FEA works at room temperature. A proposed FEA configuration for RF sources was developed by Charles Spindt et al. at SRI International and is referred to as the Spindt Cathode [12]. The Spindt structure can be improved by considering carbon nanotubes (CNTs) as cold cathode emitters. CNTs are ideal field emitters in a Spindt-type device, so many efforts have been spent worldwide in studying their field emission properties [13][14]. The recent advances in micromachining technique, in the etching process and the availability of aligned CNTs permit the realization of devices with reduced dimension and frequency operating range in the field of the THz. The great challenge of realizing devices whose dimensions are in the 1-100 μm range requires deep knowledge of their electrical behavior and physics

CHARGE TRANSPORT THEORY

Quantum charge transport results presented in this work have been obtained by using the quantum transport simulator gDFTB [15]. In the gDFTB formalism, the self-consistent Green's functions scheme is implemented on a DFT-based tight-binding framework. The density-functional Hamiltonian matrix elements are evaluated starting from the Slater-Koster two center approximation [16]. These elements, represented on a suitable nonorthogonal atomic-like basis set, are obtained by first principle computations as a function of atomic distance and are stored. Starting from this parametrization, the matrix elements for the actual system to be simulated are simply obtained by interpolation. This approach combines an *ab initio* accuracy with a highly efficient computational method.

The self-consistent charge density approach of gDFTB is based on the expansion [17] of the electronic charge density of the system as $n(\mathbf{r}) = n_0(\mathbf{r}) + \delta n(\mathbf{r})$, where $n_0(\mathbf{r})$ is a reference density (which is chosen as the density associated to the neutrality condition, i.e., when no charge transfer occurs among the atoms of the system), and $\delta n(\mathbf{r})$ is a superimposed density variation which takes into account the local charge transfer induced by chemical bonding and eventual external fields. Starting from the expansion of the total charge density, the Kohn-Sham energy functional can be expanded up to second order in the density variation $\delta n(\mathbf{r})$ [17], obtaining

$$E[n(\mathbf{r})] = E[n_0(\mathbf{r})] + E_2[\delta n(\mathbf{r}) \cdot \delta n(\mathbf{r}')], \quad (1)$$

where E_0 represents the zeroth-order contribution, just determined by $n_0(\mathbf{r})$, and E_2 represents the second-order correction to the total energy due to the charge density variation.
Applying the variational principle to the energy functional (1), it is possible to obtain [17] a modified Hamiltonian for the Kohn-Sham equations, whose matrix representation on the tight-binding electronic states of the system is

$$H_{\mu\nu} = H^0_{\mu\nu} + H^1_{\mu\nu}, \tag{2}$$

where H^1 is the correction-shift to the standard zeroth-order Hamiltonian H^0. H^0 is the reference Hamiltonian of the neutral system, and represents the starting point of the selfconsistent cycle. The shift H^1 is instead evaluated at each step of the self-consistent procedure, and is a linear function of the first-order correction $\delta n(\mathbf{r})$ to the total charge density [18]. The exchange and correlation (XC) contributions to the total energy are considered in a local density approximation (LDA), and are included in H^1 as on-site Hubbard energies [17]. Details of this DFT-based approach and its successful applications to a large variety of organic and inorganic systems have been extensively given elsewhere [19]. Indeed, to properly treat the self-consistent quantum transport problem, we need to calculate the charge density variation $\delta n(\mathbf{r})$ starting from the Hamiltonian in Eq. 2 and taking into account the non-equilibrium carriers distribution generated by the application of a bias. The Non-Equilibrium Green Functions (NEGF) technique is used to this aim.
To apply this formalism, the CNT has to be divided into two semi-infinite reservoirs which act as source and drain contacts, and a central region which scatters the propagating electronic states incoming from the two reservoirs.
The occupation of the non-equilibrium scattering states of the system is completely resolved by knowing the density matrix $\rho_{\mu\nu}$. In the NEGF formalism, this fundamental quantity can be obtained starting just from the non-equilibrium Green's function of the system, $G^<$, as [20]

$$\rho_{\mu\nu} = \frac{1}{2\pi i}\int_{-\infty}^{+\infty} G^<_{\mu\nu}(E)dE, \tag{3}$$

We evaluate this integral by using standard methods proposed in the literature [21]. Technical details more specific to our approach can be found in Ref. [18]. Here we only limit ourselves to give some details on $G^<$, in order to give an intuitive insight in the physical meaning of the formalism. In its most general formulation, the steady-state non-equilibrium Green's function of the system is given by the Keldish- Kadanoff-Baym (KKB) equation [22], [23], [24],

$$G^<(E) = G^R(E)\Sigma^<(E)G^A(E), \tag{4}$$

where

$$G^{R(A)} = \left[ES - H - \sum_{i=1}^{M}\Sigma_i^{R(A)}\right]^{-1},$$

is the standard, equilibrium, retarded (advanced) Green's function of the system, and $\Sigma^<$ is the non-equilibrium self-energy . The quantities which appear in the expression of $G^{R(A)}$ are the
Hamiltonian matrix H, just given by Eq. 2, the overlap matrix S, resulting from the choice of a non-orthogonal tight-binding basis set, and $\Sigma^{R(A)}$ the self-energies for each of the M contacts of the device, describing the coupling of the device with the M semiinfinite reservoirs. Scattering sources, such as electron-phonon or electron-electron interaction, can be included in the general expression of $\Sigma^<$ to describe incoherent transport. The method we use in this work is restricted to the description of coherent transport mechanisms. In this case, $\Sigma^<$ is determined only by the coupling of the device with the two semi-infinite contacts, and results to be

$$\Sigma^<(E) = -2i\,\mathrm{Im}\left[\sum_{i=1}^{M} f_i \Sigma_i^R(E)\right], \tag{5}$$

The electronic states of the semi-infinite reservoir i are filled according to the Fermi distribution function f_i.
The total charge density variation $\delta n(\mathbf{r})$ needed for the selfconsistent computation of the Hamiltonian can be expressed as a superposition of atom-centered charge fluctuations, $\delta n(\mathbf{r}) = \Sigma_i\, \delta n_I(\mathbf{r})$, which, in turn, are approximated by retaining

only the monopole terms $\delta n_i(\mathbf{r}) \approx \Delta q_i\, n_i(\mathbf{r})$. The atom-centered spherical cahrge densities, $n_i(\mathbf{r})$, are s-like orbital function with exponential decay [17], and Δq_i is the variation in number of electrons for the ith atom. The key step of the self-consistent computation is just the evaluation of Δq_i. This quantity is obtained starting from the non-equilibrium density matrix ρ, via the Mulliken charge analysis [17]

$$\rho_i = \sum_{\mu\in i}\sum_{\nu} \mathrm{Re}\left[\rho_{\mu\nu} S_{\mu\nu}\right] - q_i^0, \tag{6}$$

where $S_{\mu\nu}$ are the elements of the overlap matrix and q^0 are the atomic charge of the neutral atoms.

The correction to the TB Hamiltonian can be written as $H^1_{\mu\nu} = S_{\mu,\nu}\,(V_i + V_j)/2$, where the on-site shifts, V_i, are calculated from the electrostatic potential $V(\mathbf{r})$ using the projection $V_i = \int V(\mathbf{r}) n_i(\mathbf{r}) d\mathbf{r}$. The self-consistent electrostatic potential $V(\mathbf{r})$ is in turn obtained by solving a three dimensional Poisson equation in real space using a multigrid algorithm:

$$\nabla \cdot \left[\varepsilon(\mathbf{r}) \nabla V(\mathbf{r})\right] = -4\pi \sum_i \Delta q_i n_i(\mathbf{r}), \tag{7}$$

To correctly take into account the applied bias, Dirichlet boundary conditions are used on the Poisson calculation box correspondingly to the semi-infinite contacts.
To summarize, our overall procedure consists in solving self-consistently the set of equations (2-4) coupled with the Poisson equation (7), until the computed atomic charge does not vary within a specified tolerance.
The current flowing in the system can also be computed starting from G and Σ.

$$I_i = \frac{e}{h} \int Tr\left[\Sigma_i^<(E) G^>(E) - \Sigma_i^>(E) G^<(E)\right] dE, \tag{8}$$

The expression for the coherent contribution to the current just recovers the usual expression obtained in Landauer formulation [20]

SIMULATION OF FIELD EFFECT TRANSISTORS BASED ON CARBON NANOTUBES

Here we focus our attention on the theoretical description which can be given of bulk-modulated, CNT-based field-effect transistors (CNTFETs) by means of the *gDFTB* approach. The physical mechanisms governing transport in these devices, starting from the role played by one-dimensional screening on gate- and drain-induced current modulation, can be correctly predicted at an atomistic level within our approach.
The system we have simulated is shown in Fig. 1. It consists of an infinite, semiconducting CNT (7,0), having a diameter of 5.52 Å and an energy gap $E_g = 1.3$ eV. The nanotube is coaxially gated by a metallic cylindric contact centered in the middle point of the channel. The gate length is 1.2 nm. An insulator layer with dielectric constant $\varepsilon_r = 3.9$ and a thickness of 0.8 nm surrounds the CNT.

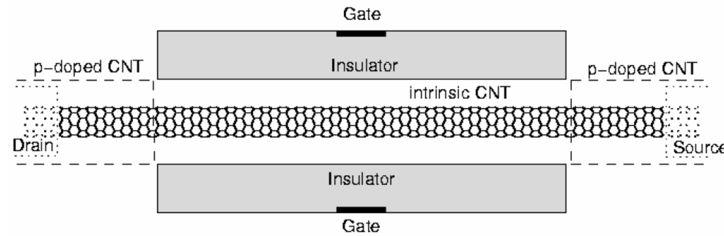

Figure 1: Schematic cross section of the coaxially gated CNTFET we have simulated.

Details on the interface between the source-drain metallic contacts and the semiconducting nanotube are not necessary in order to describe bulk-switching mechanisms, which consist of a local gate-field modulation with no electrostatic coupling with the metallic contact structures.
To simulate charge injection in the intrinsic channel, we simply dope the two ending portions of the nanotube by varying the number of valence electrons per carbon atoms [25]. Calculations have been performed retaining only the p_z-orbital part of the Hamiltonian. This is sufficient to accurately describe the first conduction and valence bands of the CNT (7,0).

In bulk-modulated CNTFETs, current modulation depends on the channel capability to screen the local gate field, that is, on the amount and the distribution of charge that can be locally induced on the CNT by the applied gate bias. Owing to their very small, one-dimensional density of states (DOS), nanotubes are generally not able to completely screen the gate field in the small extension of the electron gas associated to the graphene sheet.
In this situation, the channel charge response for a given gate bias can no longer be described by using only the geometrical capacitance of the insulator. On the contrary, a correction should be brought to the insulator capacitance to account for the correct value of the induced charge. This correction is obtained by means of the so called quantum capacitance [26]. The total capacitance of the gated nanotube system, C_Q, is given by the series connection of the geometric and the quantum capacitances [27], respectively C_{ins} and C_Q as $1/C_G = 1/C_{ins} + 1/C_Q$. A correct evaluation of the quantum capacitance is fundamental in order to correctly describe the charge response (and consequently the barrier height modulation properties) of a bulk-modulated CNTFET. The *gDFTB* approach naturally includes the treatment of the quantum capacitance, since the charge induced on the nanotube is computed self-consistently with the gate electrostatics. Furthermore, by using an atomistic, DFT-based approach, the computed charge takes into account the DOS of the one-dimensional system and retains, at least within a mean-field approximation, some of the electron-electron exchange and correlation effects on the nanotube screening properties. The importance of many-body corrections to the quantum capacitance of a gated nanotube has been recently pointed out in Ref. [28] and [29]. In large diameter tubes, where the contribution of the exchange interaction to the total energy is negligible, the quantum capacitance can be estimated simply from the DOS as $C_Q^{DOS} = e^2 \rho_0 (\varepsilon_F) L$. For small diameter tubes, due to the predominance of the exchange interaction over the kinetic energy, the quantum capacitance can instead be very different from the DOS-proportional result, and can even assume negative values. From a physical point of view, this means that the nanotube, owing to the predominance of the attractive exchange interaction among electrons, can accumulate even more charge than what strictly needed to totally screen the gate field, giving rise to a small over-screening of the gate potential in its interior.

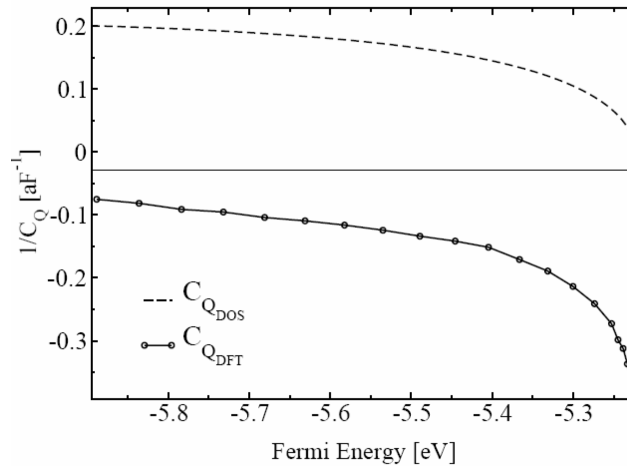

Figure 2: Computed inverse quantum capacitance of the coaxially gated CNT (7,0) as a function of the Fermi level inside the first valence subband. Solid line refers to DFT calculations. Dashed line refers to $C_Q = e^2 \rho_0 (E_F)$.

In Fig. 2 we report the computed inverse quantum capacitance of a uniformly p-doped CNT (7,0) as a function of the Fermi energy inside the first CNT valence subband. Each value of the Fermi energy univocally corresponds to a given p-doping fraction. These results have been obtained following the methodology presented in Ref. [28], and refer to an insulator capacitance C_{ins}=0.28 aF. Solid line refers to the DFT atomistic computation, while dashed line is representative of the DOS-limited, non-interacting result. The nanotube over-screens the external gate field in the whole range of holes densities we have explored, and no positive values of the quantum capacitance have been obtained.

In Fig. 3 we show the calculated output characteristics for a *p-i-p* CNTFET. The intrinsic channel of the simulated nanotube is 10.26 nm long. Source and drain contacts are *p*-doped with a carrier concentration of $2.63 \cdot 10^6$ cm^{-1}, corresponding to a doping fraction *f*=0.004 holes per carbon atom. In realistic devices, this carrier concentration can be easily obtained by an electrostatic doping, controlled by means of a back gate contact [2]. This doping causes the nanotube Fermi level to be shifted inside the first valence subband, at ~16 meV below the subband edge. Charge transfer at the junction between the degenerate *p*-type and the intrinsic portion of nanotube generates a barrier for holes transmission in valence band. The different curves shown in Fig. 3 refer to different gate biases. Positive potentials applied to the gate contact increase the barrier height for holes transmission, hence reducing the current for a given drain voltage.

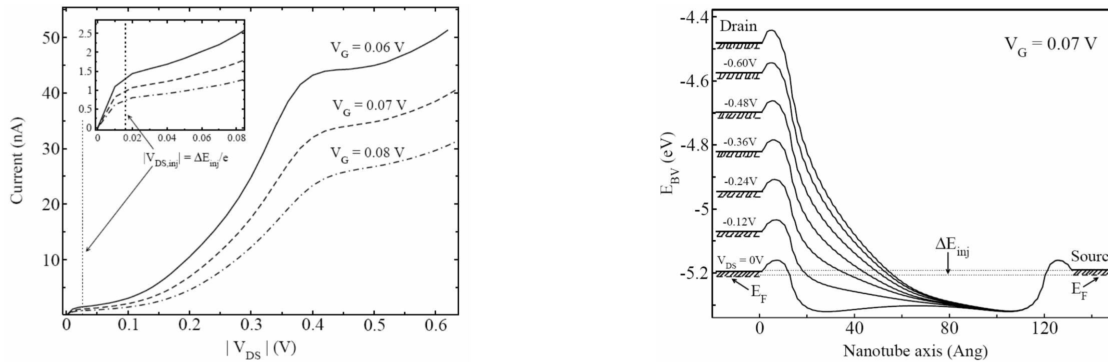

Figure 3: Computed output characteristics of the *p-i-p* CNTFET. Different curves correspond to different gate potentials. The inset shows details of the first two operative regimes of the device, the linear regime and the carrier injection saturation. The corresponding band profiles are shown in right panel.

The physical mechanisms governing the current dependence on the applied source-drain bias can be understood referring to the band profiles shown in Fig. 3 (right). These band profiles have been obtained, for a fixed gate potential, by varying the drain-source applied bias, V_{DS}, in a range of negative values (as required for a *p*-type conduction device).

The current is determined by the holes transmission probability in the energy interval between the Fermi levels of the source and drain contact. Although the applied bias continuously shifts the drain Fermi level with respect to the source, the nanotube bandgap reduces the energy window for hole injection to the energy interval ΔE_{inj}, between the source valence band edge and the source Fermi level (see Fig. 3). In other words, the maximum holes injection in the channel is fixed by the source doping rate.

At first, current linearly increases as a function of the applied bias, simply due to the increasing of the energy window for carrier injection between the source and drain Fermi levels. As the maximum energy window for carrier injection is reached, corresponding to the bias $|V_{DS,inj}| = \Delta E_{inj} / e$ (see also the inset of Fig. 3), the current does not completely saturate due to a drain-induced modulation of the barrier width within the fixed injection interval, which considerably increases the holes transmission probability. It should be kept in mind that the fundamental reason for the behavior we observe is that the device operates in such a regime that current is entirely due to tunneling through the potential barrier.

In purely ballistic devices, it is just the barrier height which determines the device behavior. On the contrary, in tunneling regimes, also the barrier width and shape are relevant in determining the current. In the *p-i-p* structure we have simulated, the contact Fermi level lies closely to the valence subband edge, well below the top of the potential

barrier for hole transmission (see Fig. 3). This is not totally unexpected for a small-diameter nanotube junction, where charge transfer occurring at the doped-intrinsic interface is distributed over an exiguous number of carbon atoms, owing to the marked quasi-one dimensionality of the system. A large shift in the atomic energy can therefore results also from a relatively small charge transfer, causing a very high potential barrier with respect to carrier injection level. This deeply differentiates the behavior of a CNTFET with respect to the ballistic transport theory developed for silicon nano-MOSFET [30]. The strong dependence of the saturation current on the drain bias we have so far observed, is just caused by the exponential dependence of the tunneling current on the width of the barrier. We can refer to the mechanism responsible for the non-saturation of the current as drain-induced barrier thinning (DIBT).

Finally, it should be noted that the short length of the channel enhances the sensitivity of the tunneling current to drain-induced barrier modulation. Longer nanotubes are therefore expected to show a considerably lesser sensitivity of the saturation current to the drain bias. In Fig. 4 we show the trans-characteristic obtained for the *p-i-p* CNTFET for a fixed drain bias of -0.4 V.

Simulation results show the exceptional transport characteristics of bulk-modulated CNTFETs. Firstly, we note that the device shows a perfectly unipolar behavior. Current is carried only by holes which are injected from the p-doped source contact, and is progressively switched-off by increasing the barrier for holes transmission with the gate bias. The non-monotonic behavior that can be observed in the trans-characteristic when a high gate voltage is applied is associated to band-to-band (BTB) tunneling mechanisms, which allows holes to propagate from the valence subband of source contact into the conduction band in the middle of the channel, and then to be collected into the valence subband of the drain [31] (see the inset in Fig. 4). Thanks to their intrinsic unipolar behavior, vertically scaled CNTFETs accomplish one of the fundamental requirements for a high-performance device which can be used in CMOS-like logic circuits.

The computed output-characteristics show also a very high I_{on}/I_{off} ratio, ~10^8, which is evidence of the exceptional effectiveness of the bulk-switching mechanism in modulating the current. Exceptional performances have also been obtained concerning the sub-threshold swing parameter, $S = dV_G / d(logI_{DS})$, which measures the effectiveness of the gate bias in switching off the current in the sub-threshold regime. The computed output characteristic shows a very good value for the inverse sub-threshold slope, 75 mV/dec. Note that the BTB branch of the characteristic in Fig. 4 shows a sub-threshold swing of 42 mV/dec, which is even lower than the minimum value attainable for any conventional silicon MOSFET at room temperature, which is $K_B Tln(10)/e = 60$ mV/dec.

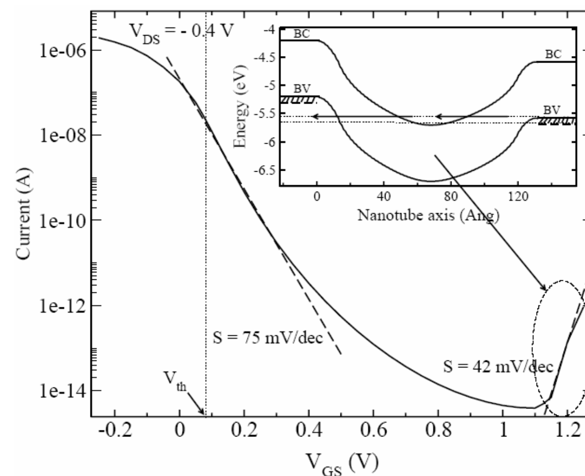

Figure 4: Trans-characteristic of a *p-i-p* CNTFET consisting of the semiconducting CNT (7,0) doped at the contacts with 0.004 holes per carbon atom. The non-monotonic behavior of the current for high gate voltages is associated to band-to-band tunneling.

FIELD EMISSION OF CNT

The gDFTB method can be applied to determine the charge density profile in the CNT used as field emitter. In the following we consider a CNT cathode in a diode configuration. Here we do not calculated the field emitted current but only the influence of the electric field on the charge density of the CNT. Also in this case, the Green approach is important since it allows for a proper account of boundary conditions (semi-infinite CNT).

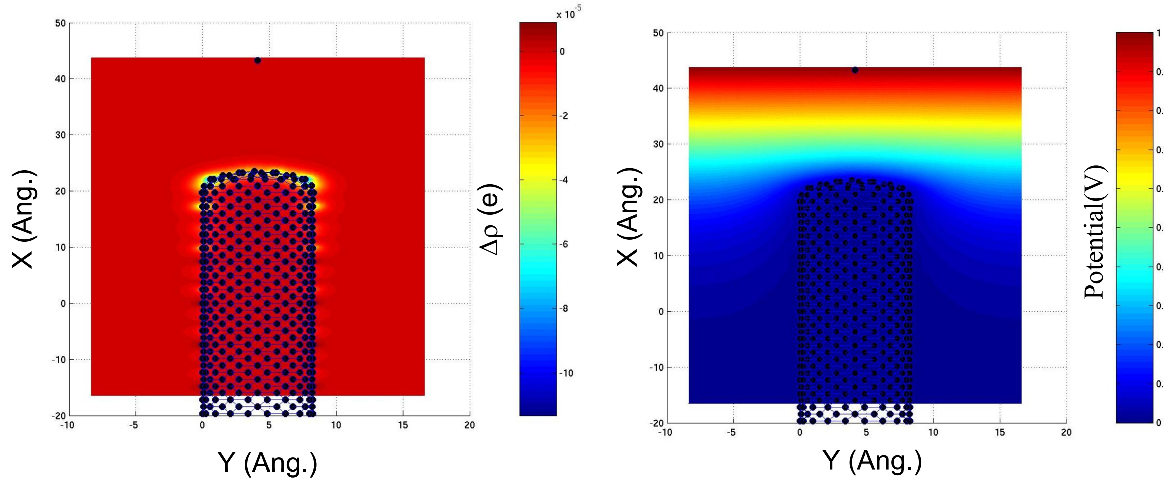

Figure 5: Charge density profile (with respect to equilibrium density) and potential profile of a (6,6) capped CNT field emitters.

Figure 5 shows both the charge profile and the potential profile for a (6,6) capped CNT with an anode potential of 1.0V Here the CNT is the cathode and the anode is 2 nm above the CNT tip. Charge oscillations in the CNT, induced by the electric field, extends over the first 4 nm of the CNT tip. Those oscillations, however, have little influence on the potential profile shown in the right side of Fig. 5

MODELLING OF THZ SOURCES BASED ON CNTS.

Triode RF amplifier structure based on CNT has been simulated by using a particle-in-cell technique coupled to a Electromagnetic simulator [32]. CNT is assumed as a cylinder with a cap of 10nm radius and 1µm in height. The triode structure is based on a typical Spindt-type field emitter triode (Fig. 6**)**. An anode plate is located 1µm away from the CNT. Other simulation parameters are: anode-gate distance, d_{ag}=0.9µm; gate radius, r_g=160nm; gate thickness, t_g=0.1µm. The emission process is modeled by the Fowler-Nordheim equation, where CNT's work function value is fixed at 4.8eV [33, 34].
The dc characteristic is obtained, observing the anode current (I_a) as a function of gate voltage (V_g) and anode voltage (V_a). The results agree with the experimental data shown in [32, 35].
The anode current as a function of anode voltage is shown in fig. 7.

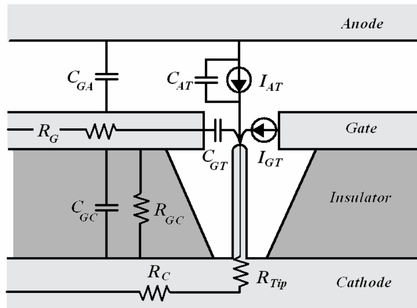

Fig 6. Equivalent circuit of the CNT triode [36]

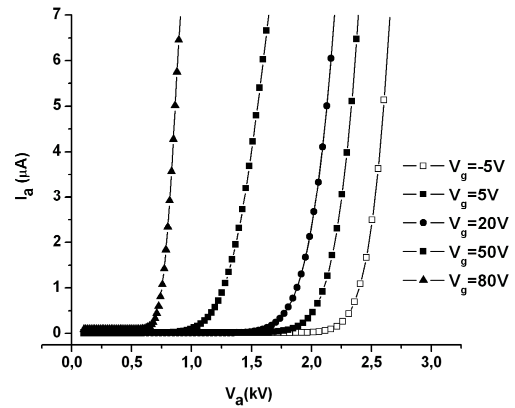

Fig 7. Output characteristics of the CNT triode

As well known, the gate electrode influences the modulation and the focalization of the electronic beam. Although a negative gate voltage of −5V is applied, an anode current is observed. In this case, the gate electrode doesn't intercept the emitted current that travels towards the anode. If the gate voltage is positive, the beam is less focalized; so the gate can collect a fraction of the emitted electrons.

The presence of this leakage current quantifies the transparency coefficient, an important triode parameter, expressed as: $T=I_A/I_{emiss}$, where I_{emiss} is the emission current from the nanotube's tip. Fig. 8 shows the results for the transparency coefficient as function of gate voltage for well aligned CNT.

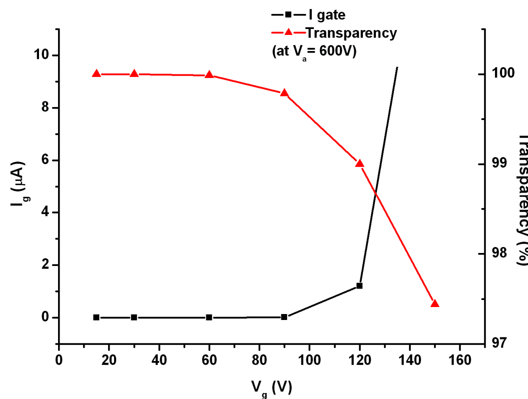

Fig. 8. Trans-characteristics of the CNT-triode and transparency

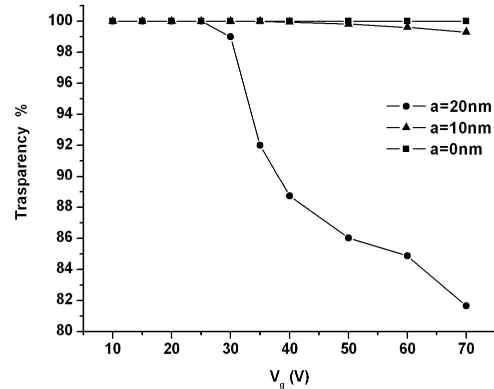

Fig. 9. Transparency as a function of CNT position

Transparency is 100% for low voltage gate while, for high positive gate voltage, the transparency is only reduced to 97.5%. The misalignment (*a*) between the centre of the nanotube and the centre of the gate hole is also studied. Simulations were done for different gate voltages, with a fixed anode voltage of 800V and gate hole radius of 160nm. Fig. 9 shows variations of the transparency coefficient as a function of three different values of misalignment parameter *a*. It can be observed no significant variation of the transparency coefficient for moderate misalignment values, while a relevant degradation of the transparency is observed for large misalignment. This is due to a larger part of emitted current intercepted by the grid and, therefore, to an increase of the leakage current.

The frequency behavior of the field emission triode with one centered CNT is plotted in Fig. 10 showing the simulated ac current gain (triode is biased at V_a = 800V, V_g=80V). The field emission triode presents a low-pass filter behavior and the cut-off frequency f_β of 37 THz.

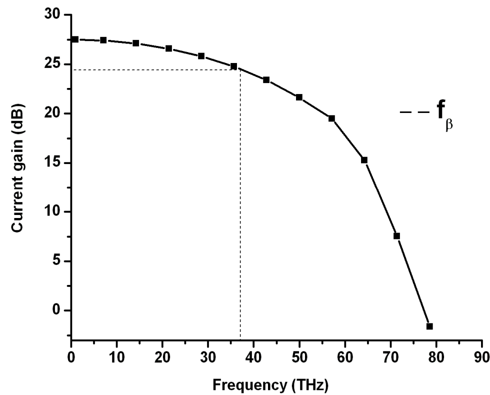

Fig. 10. Frequency behaviour of CNT-Triode

In conclusion a vacuum triode has been presented and simulated. The discussion on the principal merit factors (leakage current, transparency and cut-off frequency) demonstrate the ability of the devices to be used in the THz frequency applications[37].

ACKNOWLEDGMENTS

We acknowledge partial support of SELEX S.I. and Italian Ministry of University and Research under PRIN 2004 contract.

REFERENCES

1. J. Chen, C. Klinke, A. Afzali, and P. Avouris, *Appl. Phys. Lett.*, vol. 86, p. 123108, 2005.
2. Y. M. Lin, J. Appenzeller, J. Knoch, and P. Avouris, *cond-mat/0501690*, 2005.
3. P. L. McEuen, M. S. Fuhrer, and H. Park, *IEEE Trans. Nanotechnol.*, vol. 1, p. 78, 2002.
4. J. Appenzeller, J. Knoch, V. Derycke, R. Martel, S.Wind, and P. Avouris, *Rep. Prog. Phys.*, vol. 67, p. 1, 2004.
5. Z. Yao, C. L. Kane, and C. Dekker, *Phys. Rev. Lett.*, vol. 84, p. 2941, 2000.
6. J. Park, S. Rosenblatt, Y. Yaish, V. Sazanova, H. Ustunel, S. Braig, T. A. Arias, P. W. Brouwer, and P. L. McEuen, *NanoLett.*, vol. 4, p. 517, 2004.
7. S. T. Tans, A. R. M. Verschueren, and C. Dekker, *Nature*, vol. 393, p. 49, 1998.
8. S. Heinze, J. Tersoff, R. Martel, V. Derycke, J. Appenzeller, and P. Avouris, *Phys. Rev. Lett*, vol. 89, p. 106801, 2002.
9. M. Radosavljevic, S. Heinze, J. Tersoff, and P. Avouris, *Appl. Phys.Lett.*, vol. 83, p. 2435, 2003.
10. J. Guo, S. Datta, and M. Lundstrom, *IEEE Trans. Electron Devices*, vol. 51, p. 172, 2004.
11. Y. M. Lin, J. Appenzeller, and P. Avouris, *Nano Lett.*, vol. 4, p. 947, 2004.
12. C.A. Spindt, I. Brodie, L. Humphrey, E.R. Westerberg, J. Appl. Phys. 47, 1976
13. J.M. Bonard, H. Kind, T. Stockli , L.O. Nilsson, Solid-State Electronics 45, 2001, 893
14. Y. Vheng, O. Zhou, C.R. Physique 4, 2003, 1021
15. A. Pecchia and A. Di Carlo, *Rep. Prog. Phys.*, vol. 67, p. 1, 2004.
16. J. C. Slater and G. F. Koster, “Simplified lcao method for the periodic potential problem,” *Phys. Rev.*, vol. 94, p. 1498, 1954.
17. M. Elstner, D. Porezag, G. Jungnickel, J. Elsner, M. Haugk, T. Frauenheim, S. Suhai, and G. Seifert, *Phys. Rev. B*, vol. 58, p. 7260, 1998.
18. A. Di Carlo, A. Pecchia, L. Latessa, T. Fraunheim, and G. Seifert, *Introducing molecular electronics*. New York: Springer-Verlag, 2005.
19. T. Frauenheim, G. Seifert, M. Elstner, T. Niehaus, C. Koehler, M. Amkreutz, M. Sternberg, Z. Hajnal, A. Di Carlo, and S. Suhai, *J. Phys.: Condens. Matter*, vol. 14, p. 3015, 2002.
20. S. Datta, *Electronic Transport in Mesoscropic Systems*. Cambridge: Cambridge University Press, 1995.

21. M. Brandbyge, J. L. Mozos, P. Ordejon, J. Taylor, and K. Stokbro, “Density-functional method for nonequilibrium electron transport,”*Phys. Rev. B*, vol. 65, p. 165401, 2002.
22. L. P. K. G. Baym, *Quantum Statistical Mechanics*. Menlo Park: Benjamin, 1962.
23. L. V. Keldysh, *Sov. Phys. JEPT*, vol. 20, p. 1018, 1965.
24. P. Danielewicz, *Ann. Phys.*, vol. 152, p. 239, 1984.
25. F. Leonard, J. Tersoff: Phys. Rev. Lett. 83, 5174 (1999)
26. S. Luryi: Appl. Phys. Lett 52, 501 (1988)
27. M. Büttiker, J. Phys.: Condens. Matter 5, 9361 (1993)
28. L. Latessa, A. Pecchia, A. Di Carlo, P. Lugli, Phys. Rev. B 72, 035 455 (2005)
29. M.M. Fogler: Phys. Rev. Lett. 94, 056 405 (2005)
30. K. Natori: J. Appl. Phys. 76, 4879 (1994)
31. J. Appenzeller, Y.M. Lin, J. Knoch, P. Avouris: Phys. Rev. Lett. 93, 196 805 (2004)
32. B. Goplen, L. Ludeking, D. Smithe and G. Warren, MAGIC User’s Manual, MCR/WDC-R-409, 1997.
33. R.H. Fowler and L. Nordheim, Electron emission in intense electric fields, Proc. Roy Soc., pp. 173-181, 1928.
34. W. Zhu, C. Bower, O. Zhu, G. Kochanski and S. Jin, Appl. Phys. Lett. 75, 1999, p.873.
35. Y.M. Wong, W.P. Kang, J.L. Davidson, W. Hofmeister, S. Wei and J.H. Huang, Device characterization of carbon nanotubes in diode and triode configurations,Diamond Relat. Materials, 14, pp.697-703, 2005.
36. Jung Hyun Nam et al. J. Vac. Sci. Technol. B 16 (2), 916 (1998)
37. F.Brunetti, et al. Towards the realization of multielectrode field emission device : controlled growth of single walled carbon nanotube arrays SPIE -Microtechnologies for the New Millenium 9-11 May(2005)